



## Research article

# Characterization of a G2M checkpoint-related gene model and subtypes associated with immunotherapy response for clear cell renal cell carcinoma

Zhenwei Wang<sup>a,1</sup>, Zongtai Zheng<sup>a,1</sup>, Bangqi Wang<sup>a,1</sup>, Changxin Zhan<sup>a,b</sup>,  
Xuefeng Yuan<sup>a,c</sup>, Xiaoqi Lin<sup>a</sup>, Qifan Xin<sup>a</sup>, Zhihui Zhong<sup>d,\*</sup>, Xiaofu Qiu<sup>a,b,c,\*\*</sup>

<sup>a</sup> Department of Urology, Guangdong Second Provincial General Hospital, Guangzhou, 510317, China

<sup>b</sup> The Affiliated Guangdong Second Provincial General Hospital of Jinan University, Guangzhou, 510317, China

<sup>c</sup> The Second School of Clinical Medicine, Southern Medical University, Guangzhou, 510515, China

<sup>d</sup> Center of Stem Cell and Regenerative Medicine, Gaozhou People's Hospital, Gaozhou, 525200, Guangdong, China

## ARTICLE INFO

## Keywords:

Clear cell renal carcinoma  
G2M checkpoint  
Cell cycle  
Immune infiltration  
Drug sensitivity

## ABSTRACT

Clear cell renal cell carcinoma (ccRCC) presents challenges in early diagnosis and effective treatment. In this study, we aimed to establish a prognostic model based on G2M checkpoint-related genes and identify associated clusters in ccRCC through clinical bioinformatic analysis and experimental validation. Utilizing a single-cell RNA dataset (GSE159115) and bulk-sequencing data from The Cancer Genome Atlas (TCGA) database, we analyzed the G2M checkpoint pathway in ccRCC. Differential expression analysis identified 45 genes associated with the G2M checkpoint, leading to the construction of a predictive model with four key genes (E2F2, GTSE1, RAD54L, and UBE2C). The model demonstrated reliable predictive ability for 1-, 3-, and 5-year overall survival, with AUC values of 0.794, 0.790, and 0.794, respectively. Patients in the high-risk group exhibited a worse prognosis, accompanied by significant differences in immune cell infiltration, immune function, TIDE and IPS scores, and drug sensitivities. Two clusters of ccRCC were identified using the "ConsensusClusterPlus" package, cluster 1 exhibited a worse survival rate and was resistant to chemotherapeutic drugs of Axitinib, Erlotinib, Pazopanib, Sunitinib, and Temozolomide, but not Sorafenib. Targeted experiments on RAD54L, a gene involved in DNA repair processes, revealed its crucial role in inhibiting proliferation, invasion, and migration in 786-O cells. In conclusion, our study offers valuable insights into the molecular mechanisms underlying ccRCC, identifying potential prognostic genes and molecular subtypes associated with the G2M checkpoint. These findings hold promise for guiding personalized treatment strategies in the management of ccRCC.

\* Corresponding author. Center of Stem Cell and Regenerative Medicine, Gaozhou People's Hospital, No. 89, Xiguan Road, Gaozhou, Guangdong, Gaozhou 525200, Guangdong, China.

\*\* Corresponding author. Department of Urology, Guangdong Second Provincial General Hospital, No.466 Xingang Middle Road, Haizhu District, Guangzhou, 510317, Guangdong, China.

E-mail addresses: [zhzhong84@163.com](mailto:zhzhong84@163.com) (Z. Zhong), [xfqiu123@163.com](mailto:xfqiu123@163.com) (X. Qiu).

<sup>1</sup> Co-first authors contributed equally to this work.

<https://doi.org/10.1016/j.heliyon.2024.e29289>

Received 6 February 2024; Received in revised form 28 March 2024; Accepted 4 April 2024

Available online 5 April 2024

2405-8440/© 2024 The Authors. Published by Elsevier Ltd. This is an open access article under the CC BY-NC-ND license (<http://creativecommons.org/licenses/by-nc-nd/4.0/>).

## 1. Introduction

Pathological classification divides renal cell carcinoma into several subtypes, including kidney renal clear cell carcinoma (KIRC), chromophobe cell carcinoma, papillary carcinoma, collecting duct carcinoma, and undifferentiated carcinoma. Among them, KIRC is characterized by the presence of clear cells within the tumor, which can be observed under a microscope, and is the most prevalent subtype accounting for approximately 70–80% of cases around the world [1]. This subtype often poses a challenge for early diagnosis due to the absence of obvious symptoms in the initial stages. ccRCC is known for its aggressive growth pattern and high potential for metastasis, leading to a poor prognosis for patients [2]. Traditional treatment options such as radiotherapy and chemotherapy are typically ineffective against ccRCC, emphasizing the importance of radical nephrectomy as the primary treatment approach [3,4]. However, even with surgical intervention, a significant proportion of ccRCC patients experience distant metastases, as the surgery may not eliminate all tumor cells. Consequently, approximately 20–30% of patients may encounter metastatic recurrence following surgery, resulting in a diminished postoperative prognosis. While efforts have been made to explore the use of kinase inhibitors like sorafenib and sunitinib in clinical trials, these treatments have encountered challenges [5]. Though some kinase inhibitors like sorafenib and sunitinib have been used in clinical trials, concerns have arisen regarding their adverse effects and unexpected loss of efficacy, possibly stemming from off-target effects [6]. Therefore, gaining a comprehensive understanding of the biological characteristics of KIRC and identifying prognostic markers for renal cancer has profound implications for its diagnosis and treatment.

The G2M checkpoint pathway is an important mechanism that regulates cell cycle progression, specifically the transition from the G2 phase to the mitotic (M) phase. This checkpoint ensures that DNA replication is complete and accurate and that any DNA damage or replication errors are repaired before cells enter mitosis [7]. Dysregulation or malfunctioning of the G2M checkpoint pathway can have significant implications for the development and progression of cancer [8]. In normal cells, the G2M checkpoint pathway includes several key proteins and signaling pathways that work together to monitor DNA integrity and cell cycle progression [9]. One of the central regulators of this checkpoint is the tumor suppressor protein p53. When DNA damage or errors are detected, p53 is activated and halts cell cycle progression to allow for DNA repair. If the damage is irreparable, p53 can initiate programmed cell death (apoptosis) to eliminate the damaged cell [10]. The G2M checkpoint pathway has been reported involved in various cancers such as melanoma, breast cancer, gastric cancer, and pancreatic cancer, mutations or alterations in the genes involved in the G2M checkpoint pathway can disrupt its normal function [11–14]. This can result in the loss of cell cycle control, allowing cells with damaged DNA to continue dividing and proliferating. Mutations in p53, for example, are commonly observed in many types of cancer and are associated with defective G2M checkpoint function. In these cases, cells may bypass the checkpoint and enter mitosis despite having DNA damage, leading to the accumulation of genetic abnormalities and potentially promoting tumor growth [15]. Additionally, other proteins involved in the G2M checkpoint pathway, such as cyclins, cyclin-dependent kinases (CDKs), and checkpoint kinases, can also be altered in cancer [11]. Changes in the levels or activity of these proteins can disrupt normal cell cycle regulation, leading to uncontrolled cell division and tumor formation [16]. Moreover, high G2M checkpoint scores are consistently associated with worse overall survival and lower drug sensitivity in pancreatic cancer [12,17]. Understanding the relationship between the G2M checkpoint pathway and cancer is crucial for developing targeted cancer therapies. Researchers are investigating various strategies to restore or enhance the function of the G2M checkpoint pathway in cancer cells, intending to induce cell cycle arrest or apoptosis in cancer cells specifically, while sparing normal cells [18–20]. These approaches hold promise for the development of more effective and selective cancer treatments in the future.

To investigate and evaluate the predictive significance of the G2M checkpoint in clear cell renal cell carcinoma (ccRCC), we conducted a comprehensive bioinformatics analysis. This analysis involved the creation of a predictive prognostic gene signature associated with the G2M checkpoint by utilizing both single-cell and bulk sequencing data. We also analyzed the independence of the constructed model. Gene Ontology (GO), Kyoto Encyclopedia of Genes and Genomes (KEGG), and immune infiltration enrichment were applied to shed light on the underlying mechanisms. Furthermore, we examined the correlation between risk scores and drug sensitivities, providing valuable insights into potential therapeutic implications. By identifying distinct subtypes, we aimed to gain a deeper understanding of the relationship between the G2M checkpoint and ccRCC.

## 2. Methods and materials

### 2.1. Data collection

We retrieved bulk-sequencing data and associated clinical information from the KIRC program, which included 537 patients and 71 control subjects from The Cancer Genome Atlas (TCGA) database (<https://portal.gdc.cancer.gov/>). For our analysis, three G2M checkpoint pathways: BIOCARTA\_G2\_PATHWAY, HALLMARK\_G2M\_CHECKPOINT, and REACTOME\_G2\_M\_CHECKPOINTS were sourced from the MsigDB database (<https://www.gsea-msigdb.org/gsea/msigdb>). A total of 354 unique genes associated with the G2M checkpoint were retained for further investigation.

### 2.2. Enrichment analysis of G2M pathway in ccRCC

In order to investigate the activity of the G2M checkpoint pathway in a single-cell dataset, we searched KIRC-related genesets within the TISCH database (<http://tisch.comp-genomics.org/home/>). The dataset GSE159115, comprising eight patients and generated using 10x genomics, yielded a total of 27,669 cells. To analyze and visualize the single-cell signature explorer, we utilized the gene set enrichment analysis (GSEA) function available on the aforementioned website. We utilized the 'clusterProfiler' package for

enrichment analysis of G2M checkpoint pathways in the bulk-sequencing data. The results were then visualized using the 'ggplot2' package.

Identification and construction of prognostic signature based on differentially expressed G2M checkpoint-related genes.

The expression data of the selected 354 genes were extracted and subjected to analysis using the "limma" package in order to identify genes that were differentially expressed between the tumor and control samples. Genes meeting the criteria of a false discovery rate (FDR) < 0.05 and  $|\log \text{fold change (FC)}| > 1$  were considered as differentially expressed genes (DEGs). The DEGs associated with the G2M checkpoint were then extracted and visualized through a heatmap generated using the "pheatmap" R package. Subsequently, the remaining genes were subjected to univariate Cox regression analysis to identify prognostic genes associated with overall survival (OS). To mitigate the risk of overfitting, we employed Lasso Cox regression analysis to eliminate genes prone to overfitting and construct a predictive model using the "glmnet" R package. The risk score for each patient was calculated using the following formula:

$$\text{Risk score} = \sum_{i=1}^n \text{Coef}(\beta_i) * \text{Exp}(X_i)$$

The coefficients ( $\beta_i$ ) represent the calculated coefficient values of the model gene obtained from Lasso Cox regression, while  $\text{exp}(X_i)$  denotes the expression level of the model gene. The patients from the TCGA-KIRC dataset were randomly and equally divided into training and testing cohorts. In both cohorts, patients were categorized into either a high-risk or low-risk group based on the median risk score of the derivation set. To visualize the distribution patterns, scatter diagrams were created using the "pheatmap" R package to display the risk scores and corresponding survival times of all patients. The gene expression of the established signature was analyzed using principal component analysis (PCA) with the "stats" R package. Furthermore, the patients in different risk groups were visualized using t-distributed stochastic neighbor embedding (t-SNE) with the "Rtsne" R package. Kaplan-Meier (K-M) survival analysis and time-dependent receiver operating characteristic (ROC) analysis based on OS were performed to assess the prognostic accuracy of the gene signature. This analysis utilized the "survival" package, the "survminer" package, and the "timeROC" package in R. The gene signature's prognostic accuracy was evaluated in the training and testing sets.

### 2.3. Verification of the model's independence and construction of a nomogram

To further confirm whether the constructed model is a factor independent from other clinical characteristics of age, gender, and TNM stage for predicting OS. We conducted univariate and multivariate Cox regression by "survival" package to assess hazard ratios (HRs) and 95% confidence intervals (CIs).

By integrating risk scores with clinical pathological factors, we utilized the "rms" package to generate line graphs depicting the 1-, 3-, and 5-year O rates for ccRCC patients. These line graphs provided a visual representation of how the risk scores, in conjunction with clinical pathological factors, influenced OS over different time intervals. To demonstrate the predictive capability of the developed nomogram models, we employed the calibration curve. This curve served as a graphical representation of the model's performance, showcasing how well the predicted probabilities aligned with the actual outcomes. To assess the accuracy of the model, we utilized the consistency index (C-index) to discriminate between different outcomes, providing a measure of its overall accuracy.

### 2.4. Functional annotation analysis

To investigate the potential functional annotation and pathways associated with the risk groups, we utilized the 'limma' R package to identify DEGs between the risk groups, and the low-risk group was set as the control. DEGs were determined based on criteria of  $|\log \text{FC}| > 1$  and  $p < 0.05$ . The "clusterProfile" package was applied to generate the Kyoto Encyclopedia of Genes and Genomes (KEGG) pathways and Gene Ontology (GO) functional annotation related to the DEGs for providing insights into the biological processes associated with the risk groups. Gene Set Variation Analysis (GSVA) represents a distinct form of gene set enrichment technique designed for individual samples. It facilitates pathway-focused investigations of molecular data by introducing a conceptually straightforward yet influential modification in the fundamental unit of analysis, shifting the focus from individual genes to sets of genes. We applied the "GSVA" package to analyze the potential pathways involved in the different clusters.

### 2.5. Calculation of immune cell infiltration, immune function, tumor immune dysfunction and exclusion (TIDE), and immune phenotype score (IPS) scores

To investigate the disparities in immune cell infiltration and immune function scores between the high-risk and low-risk groups, we first examined the levels of immune and stromal cells in each group. To quantify these differences, we utilized the ESTIMATE algorithm to compute the StromalScore, ImmuneScore, and ESTIMATEScore (StromalScore + ImmuneScore) for each group. Then, single-sample gene set enrichment analysis (ssGSEA) for immune infiltration was applied with the "GSVA" R package to assess the infiltration score of 28 immune cells and the activity of 13 immune-related functions. Furthermore, we obtained the immunotherapy data from the tumor immune dysfunction and exclusion (TIDE) website (<http://tide.dfci.harvard.edu>). It is used to evaluate the potential clinical efficacy of immunotherapy in different risk groups, reflecting the potential ability of tumor immune evasion. A higher TIDE score is associated with poor ICI efficacy. Based on the model gene expression we then evaluated MSI scores, dysfunction scores, exclusion scores, and the TIDE score (MSI scores + dysfunction scores + exclusion scores). Additionally, we acquired IPS score data for four phenotypes including *ctla4\_negative\_pd-1\_negative*, *ctla4\_negative\_pd-1\_positive*, *ctla4\_positive\_pd-1\_negative*, *ctla4\_positive\_pd-1\_positive* for ccRCC patients from the TCIA database (<https://tcia.at/>). The higher the immunophenotype score, the higher the immunotherapy response rate.

## 2.6. Association of model gene expression and drug sensitivity

The CellMiner database, a relational database tool designed for storing, querying, integrating, and retrieving molecular profile data from the NCI-60 and other cancerous cells, was utilized to obtain drugs currently undergoing clinical trials or approved by the FDA. To identify potential drugs associated with the expression of risk genes, we retained correlation values  $> 0.3$  and  $p < 0.01$ . Furthermore, we employed the "pRRophetic" package to predict the IC50 values of specific compounds sourced from the Genomic of Drug Sensitivity in Cancer (GDSC) dataset.

## 2.7. Identification of subtypes based on the GMCRGs model

The "ConsensusClusterPlus" package was utilized to apply the consensus clustering function, which resulted in unbiased and unsupervised findings. This process effectively grouped patients into subgroups based on the four GMCRGs.

## 2.8. Cell culture and transfection

We purchased the human renal cortex proximal tubule epithelial cells (HK-II) and RCC cell line (786-O) from the Chinese Academy of Sciences. The three cell lines were cultured in 1640 medium (Gibco, New York, NY, USA) supplemented with 10% fetal bovine serum (FBS) (Gibco, New York, NY, USA) under standard conditions of 37 °C, 95% humidity, and a 5% CO2 environment using a cell incubator. RAD54L-targeting siRNA constructs and si-NC (non-targeting control) were synthesized by GenePharma (Shanghai, China). Lipofectamine 3000 (Invitrogen, USA) was employed to introduce the siRNA constructs into the 786-O. The cells were harvested 48 h after transfection for further experimentation. The sequences of si-RAD54L: 5'-CCUAGUGACUCCUAGGAAATT-3', and si-NC: 5'-UUCUCCGAACGUGUCACGUTT-3', respectively.

## 2.9. RNA extraction and Real-Time quantitative Polymerase Chain Reaction (RT-PCR)

Total RNA extraction was performed using the EZBioscience kit (#EZB-RN4, Roseville, USA), and the concentration and purity of the extracted RNA were evaluated using a NanoDrop (Thermo Fisher, USA). Complementary DNA (cDNA) synthesis was carried out according to the manufacturer's protocol using the HiScript III RT SuperMix for qPCR from Vazyme (#R323-01, Nanjing, China). For qPCR analysis, the ChamQ Universal SYBR qPCR kit (#Q311-02, Vazyme, Nanjing, China) was utilized on the 7500 Real-Time PCR System (Thermo Fisher, USA). The relative mRNA levels were determined using the  $2^{-\Delta\Delta CT}$  method, with GAPDH serving as the internal reference. Primers for RAD54L and GAPDH were synthesized by Sangon Biotech (Shanghai, China). The primer sequences for RAD54L and GAPDH were as follows:

RAD54L Forward 5'-TTTACGCCAGAGTCCAGAGTG-3', RAD54L Reverse 5'-ATGAAGCGGAAGGTCTCATA-3', GAPDH Forward 5'-GGAGCGAGATCCCTCCAAAAT-3', GAPDH Reverse 5'-GGCTGTTGTCATACTTCTCATGG-3'.

## 2.10. CCK-8 assay

Cells were seeded in 96-well plates at a density of 2000 cells per well, utilizing DMEM medium supplemented with 10% FBS. After a specified incubation period, 10  $\mu$ l of CCK-8 (#GK10001, GLPBIO, Montclair, CA, USA) solution was added to each well and allowed to incubate for 2 h. The absorbance values at 450 nm were then measured using a microplate spectrophotometer (ThermoFisher, USA) to determine the proliferation capacity of the transfected cells.

## 2.11. Cell apoptosis and cell cycle analysis

Cell apoptosis was evaluated using the annexin V-FITC/PI detection kit (#KGA108, KeyGen Biotech, Nanjing, China). The cells were collected and subjected to staining with annexin V-FITC and PI for 10 min. Flow cytometry analysis was performed using FACSCalibur (BD Biosciences, New Jersey, USA) to determine the rate of cell apoptosis. The obtained data regarding the apoptosis rate were quantified using FlowJo software (v10). For cell cycle analysis, transfected 786-O cells were harvested through centrifugation and subsequently fixed in 75% ethanol at 4 °C for 24 h. Following another round of centrifugation, the cells were stained with PI for 20 min, and the resulting fluorescence was measured using flow cytometry. The acquired data were processed using Modfit LT software (v5.0) for further analysis of the cell cycle distribution.

## 2.12. Cell migration and invasion

To evaluate the roles of RAD54L in the migration and invasion of 786-O, a 6.5 mm transwell (#3422, Corning Costar, NY, USA) was employed. For the migration assay,  $1 \times 10^4$  cells were seeded in the upper chamber of the transwell. In the invasion assay, the transwell chamber was pre-coated with Matrigel dissolved in ABW BIO (#0827045, Shanghai, China). The Matrigel was diluted with FBS-free medium at a ratio of 1:6, and then  $1 \times 10^5$  cells were added to the transwell chamber. After incubation, the cells that successfully traversed the insert were fixed, stained with 1% crystal violet, and subsequently photographed and counted under a visible light microscope (Nikon, Tokyo, Japan).

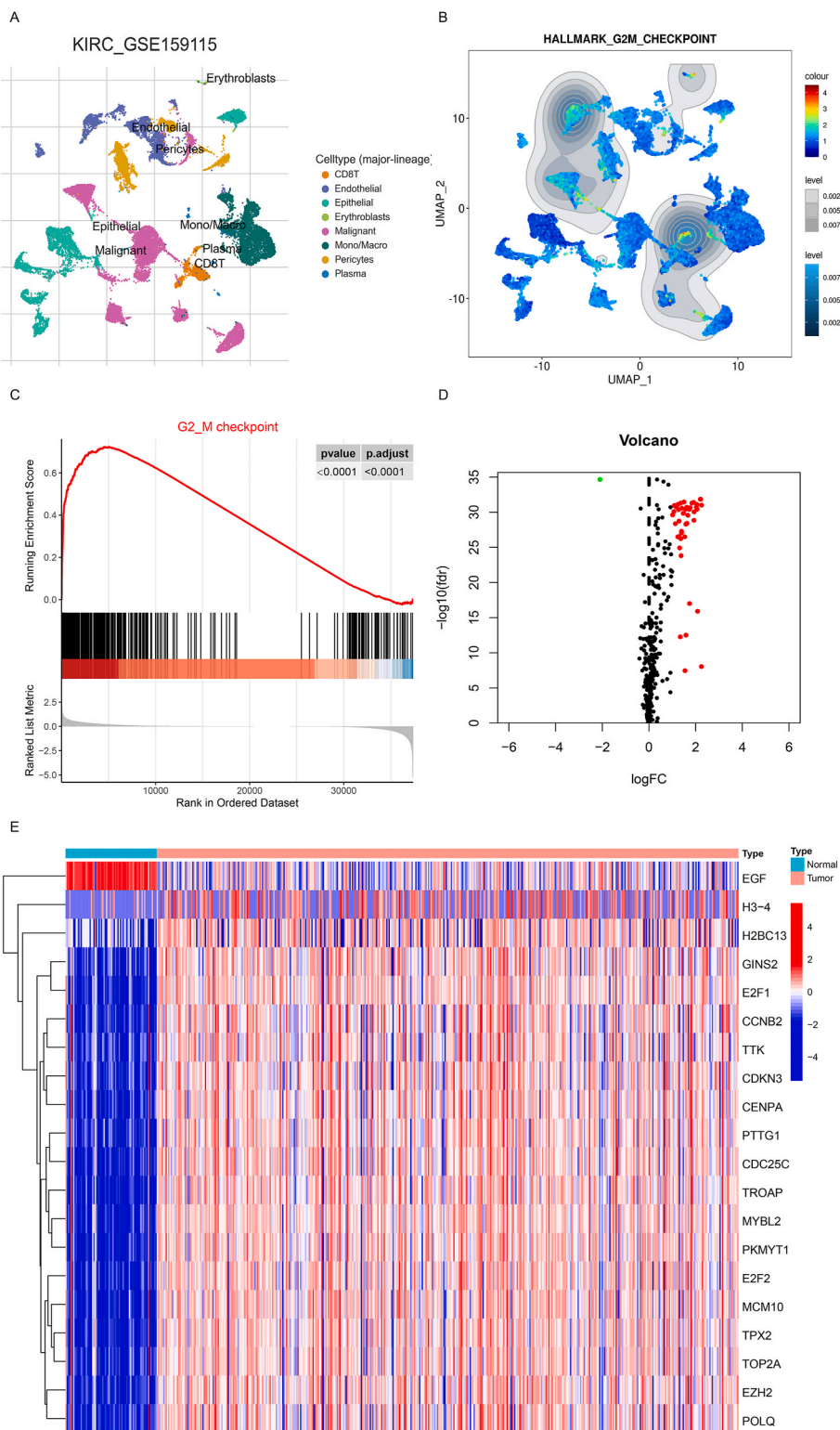


**Fig. 1. Identification of DEGs associated with G2M checkpoint.** (A) Cell types annotation of sc-RNA dataset GSE159115. (B) Distribution of G2M checkpoint pathway in sc-RNA dataset GSE159115. (C) G2M checkpoint pathway enrichment analyzed by GSEA. (D, E) Volcano and heatmap plots of G2M checkpoint-related genes, respectively. A deeper shade of red signifies a more pronounced positive correlation, while a deeper shade of blue signifies a more pronounced negative correlation. (For interpretation of the references to color in this figure legend, the reader is referred to the Web version of this article.)

2.13. Statistical analysis

Statistical analyses were conducted using R software (v4.2.0) and GraphPad Prism (v8.1). The Wilcoxon-Mann-Whitney *U* test was employed to examine the differences between the two datasets. Survival analyses were performed using the log-rank test on Kaplan-Meier survival curves to evaluate the impact of high- and low-expression risk models on patient overall survival (OS). The limma package was utilized to analyze the differential genes within the samples of two clusters of G2M checkpoint-associated genes. Statistical significance was considered when the *p*-value was less than 0.05, and the False Discovery Rate (FDR) approach was used to make nuanced adjustments for multiple comparisons.

3. Results

3.1. Identification of prognostic genes based on GMCRGs

In this study, we initially investigated the expression levels of a gene signature associated with the G2/M checkpoint in ccRCC using single-cell RNA sequencing data from the GSE159115 dataset. Through this analysis, we identified 32 clusters and 8 distinct cell types, including CD8<sup>+</sup> T cells, endothelial cells, epithelial cells, erythroblasts, malignant cells, monocytes/macrophages, pericytes, and plasma cells (Fig. 1A). As shown in the heatmap (Fig. S1) and UMAP plot (Fig. 1B), we observed that the G2/M checkpoint-related gene signature was up-regulated in tumor cells and primarily present in CD8<sup>+</sup> T cells (Cluster 1), endothelial cells (Clusters 11 and 13), malignant cells (Cluster 28), and monocytes/macrophages (Cluster 32). To further validate our findings, we performed Gene Set Enrichment Analysis (GSEA) on bulk sequencing data from the TCGA-KIRC dataset. The result demonstrated significant enrichment of the G2/M checkpoint-related gene signature in the ccRCC tumor samples (*p* < 0.0001) (Fig. 1C). These findings suggest that active G2/M checkpoint pathways may contribute to the progression of ccRCC. To gain further insights into the expression patterns of G2/M checkpoint-related genes in ccRCC, we analyzed the expression of these genes in the KIRC dataset by “limma”. We identified a total of 45 differentially expressed genes (DEGs), including 44 upregulated genes and 1 downregulated gene (Fig. 1D). The top 20 genes are depicted in the heatmap (Fig. 1E). Using these 45 DEGs, we conducted univariate Cox analysis to identify genes associated with the overall survival of ccRCC patients. A total of 36 risk factors were identified (Fig. 2A). Subsequently, we employed the LASSO Cox regression method to select featured genes for constructing a model based on G2/M checkpoint-related genes. Four genes, namely

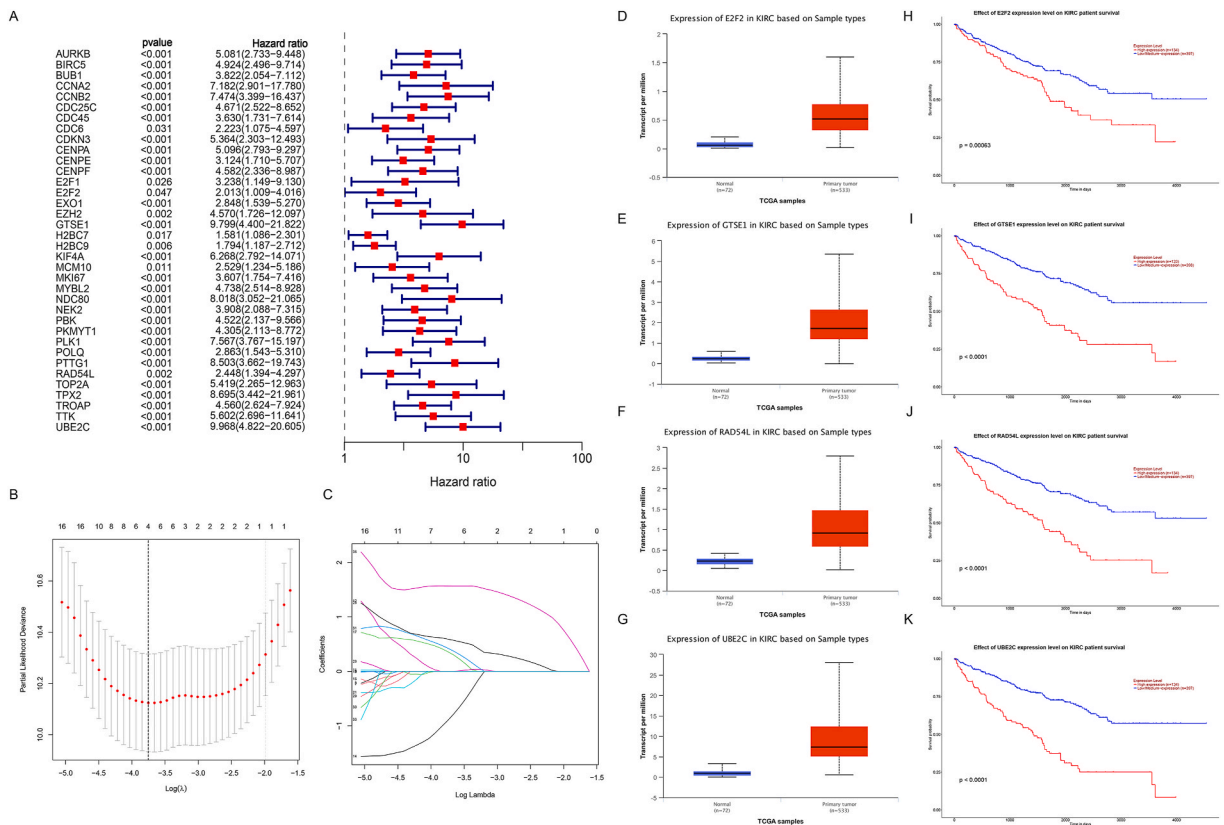


**Fig. 2.** Screening of prognostic gene for predicting OS of ccRCC based on GMCRGs. (A) Identification of prognostic genes by univariate Cox analysis. (B, C) Identification of model genes by LASSO Cox regression analysis. (D-K) Expression and survival analysis of the four model genes.

E2F2, GTSE1, RAD54L, and UBE2C, were retained in the model (Fig. 2B and C). Importantly, all four genes were upregulated in tumor tissues, and high expression of these genes correlated with poor survival outcomes for patients (Fig. 2D–K). These findings highlight the potential prognostic significance of the identified genes and suggest their involvement in ccRCC progression.

### 3.2. GMCRCGs model associates with OS of ccRCC in the training and testing cohorts

By utilizing coefficient values obtained from LASSO Cox analysis for four specific genes, we calculated a risk score for each patient using the subsequent formula:  $(-2.0736 \times E2F2) + (1.6942 \times GTSE1) + (1.6944 \times RAD54L) + (1.6099 \times UBE2C)$ . To establish distinct training and testing cohorts for the TCGA-KIRC patients, a random division was performed at a 1:1 ratio. Subsequently, based on the median risk score, the patients were categorized into high-risk and low-risk groups. In the training cohort, this classification was further supported by a dot and PCA plot, clearly distinguishing the patients into high and low-risk groups (Fig. 3A–D). Analysis of survival status demonstrated a correlation between higher risk scores and poorer prognosis (Fig. 3B). Accordingly, the K-M survival plot indicated that patients in the high-risk group experienced shorter overall survival compared to those in the low-risk group ( $p < 0.001$ ) (Fig. 3C). To evaluate the predictive capability of our prognostic model, ROC curves were employed, yielding AUC values of 0.794, 0.790, and 0.794 for 1-, 3-, and 5-year overall survival, respectively (Fig. 3E). Additionally, the expression levels of the model genes exhibited an increase corresponding to higher risk scores (Fig. 3F). Consistent outcomes were observed within the testing cohort, where patients were clearly segregated into high- and low-risk groups (Fig. S2A, D). The high-risk group exhibited an unfavorable overall survival (Fig. S2B, C). The corresponding AUC values for 1-, 3-, and 5-year overall survival were 0.772, 0.730, and 0.739, respectively (Fig. S2E). These findings strongly suggest that the prognostic model, comprising four genes associated with the G2/M checkpoint, is reliable and powerful in predicting overall survival for ccRCC patients.

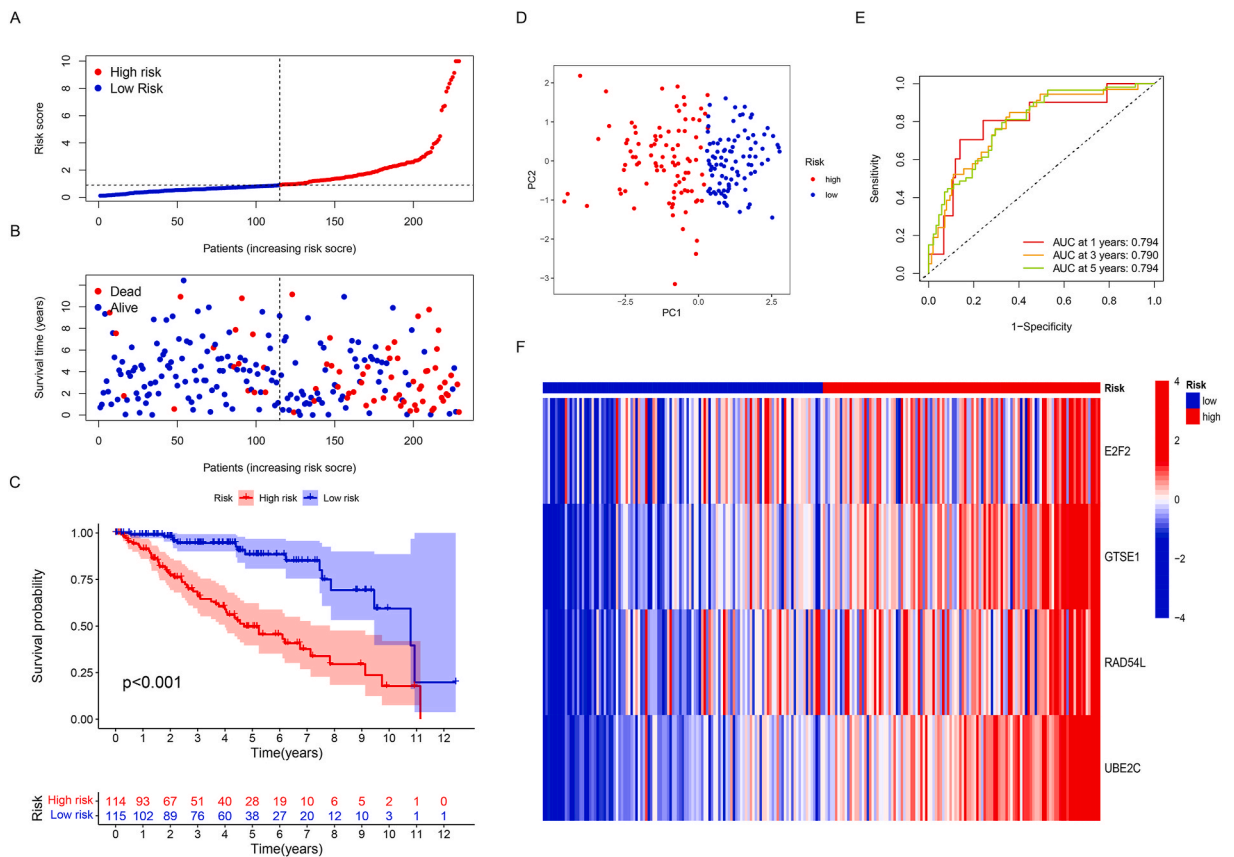


**Fig. 3. Construction of a predictive GMCRCGs model in the training cohort.** (A) Dividing patients into high- and low-risk groups by median value of risk score. (B) Distribution of patients' survival status. (C) The survival curves for OS of the high- and low-risk groups. (D) PCA plot. (E) Analyzing the ROC curve to verify the predictive performance of the model for 1-, 3-, and 5-year OS. (F) Expression levels of model genes in the high- and low-risk groups. A deeper shade of red signifies a more robust positive correlation, while a deeper shade of blue signifies a stronger negative correlation. (For interpretation of the references to color in this figure legend, the reader is referred to the Web version of this article.)

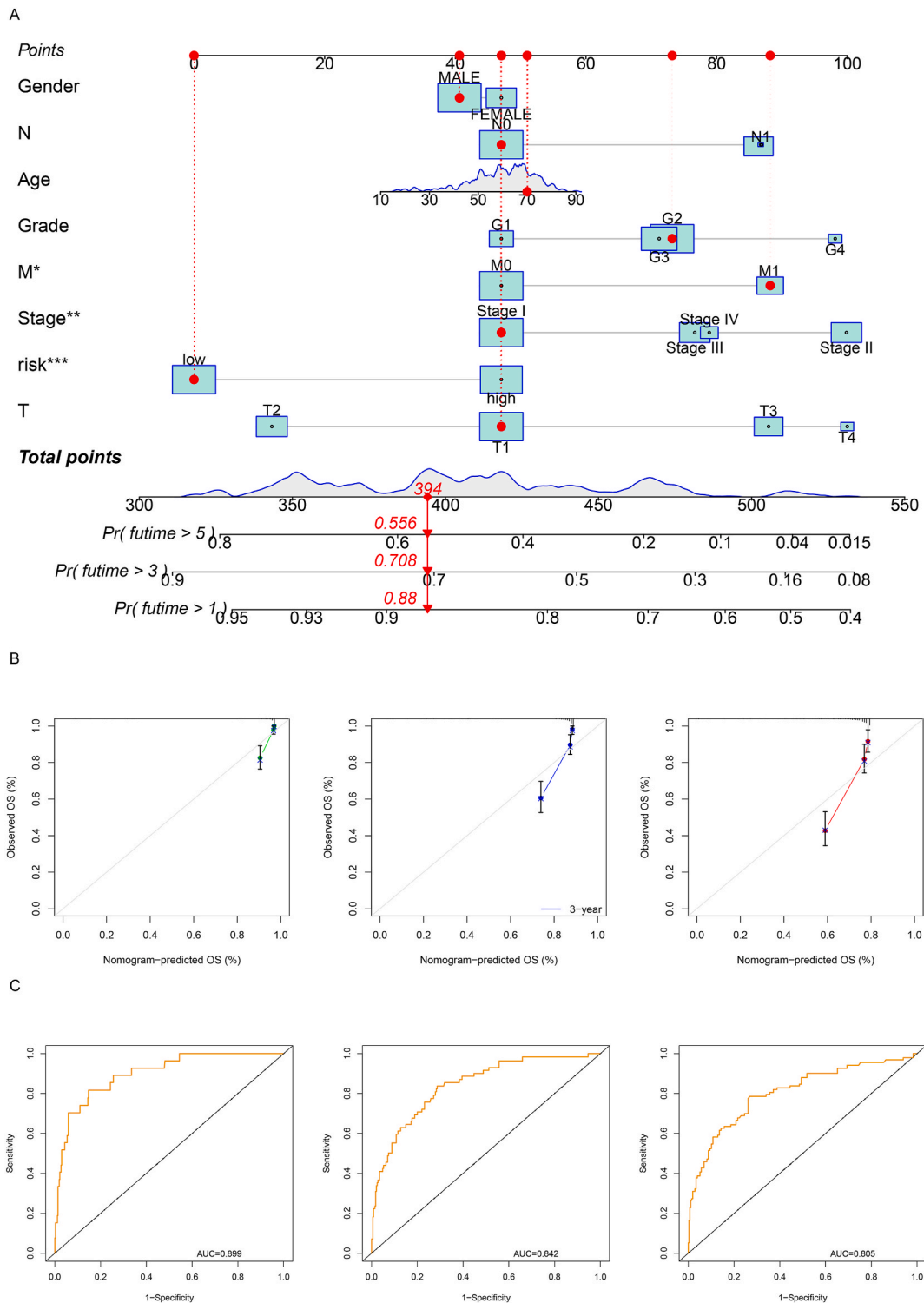


**Fig. 4. Developing a Predictive Nomogram. (A)** Utilizing clinical factors and risk scores to build a nomogram for predicting survival. **(B)** Evaluating the performance of the Nomogram for predicting 1-, 3-, and 5-year survival through ROC Curve Analysis. **(C)** Assessing the accuracy of the Nomogram in predicting 1-, 3-, and 5-year survival using calibration curve analysis.

### 3.3. GMCRGs model is an independent factor and correlates to clinical characteristics in ccRCC

We conducted univariate and multivariate Cox regression analyses to examine whether the constructed model could serve as a predictive factor independent of other clinical features such as age, gender, TNM stage, and grade. In the training cohort, both Cox regression methods consistently indicated that the model was a significant factor separate from the other clinical features. The results were as follows: univariate Cox regression: hazard ratio (HR) = 1.325, 95% confidence interval (CI) = 1.214–1.446,  $p < 0.001$ ; multivariate Cox regression: HR = 1.320, 95% CI = 1.200–1.451,  $p < 0.001$  (Fig. S3A, B). Furthermore, the outcomes from the testing cohort supported these findings. The results were as follows: univariate Cox regression: HR = 1.217, 95% CI = 1.071–1.383,  $p = 0.003$ ; multivariate Cox regression: HR = 1.170, 95% CI = 1.170–1.360,  $p = 0.04$  (Fig. S3C, D). We also conducted additional analyses to examine the correlation between the risk scores obtained from the model and various clinical features. Except for age, the risk scores exhibited significant differences between groups (Fig. S4). Notably, the risk scores demonstrated a positive association with T stages, grades, and stage levels of the prognostic model. These findings suggest that the GCRGs model is an independent factor and is closely associated with the clinical features of ccRCC.

### 3.4. Construction of a Predictive Nomogram

We developed a comprehensive nomogram to accurately predict the OS of ccRCC patients at 1, 3, and 5 years. The nomogram incorporates a risk score and several key clinical factors, namely age, chemotherapy, radiotherapy, status, and grade. Our analysis yielded a concordance index (C-index) of 0.768 for the nomogram (Fig. 4A). The calibration curves demonstrated a close match between the predicted mortality and the actual mortality rates (Fig. 4B). Furthermore, the ROC curves for the 1-, 3-, and 5-year OS displayed high levels of accuracy, with values of 0.818, 0.860, and 0.853, respectively (Fig. 4C). The findings highlight that our nomogram may be an exceptional tool for predicting survival outcomes in individuals with ccRCC.

### 3.5. GMCRGs model associated with immune cell infiltration and immunotherapy response in ccRCC

The prognosis of cancer is greatly influenced by immune cell infiltration. In this study, we analyzed to investigate the immune and stromal scores using the "ESTIMATE" method in both high- and low-risk groups. Our findings revealed that the high-risk group exhibited a higher immune score, while no significant difference was observed in the stromal score. Additionally, the ESTIMATE score was higher in the high-risk group (Fig. 5A). To further analyze immune cell infiltration in ccRCC, we applied the ssGSEA algorithm to

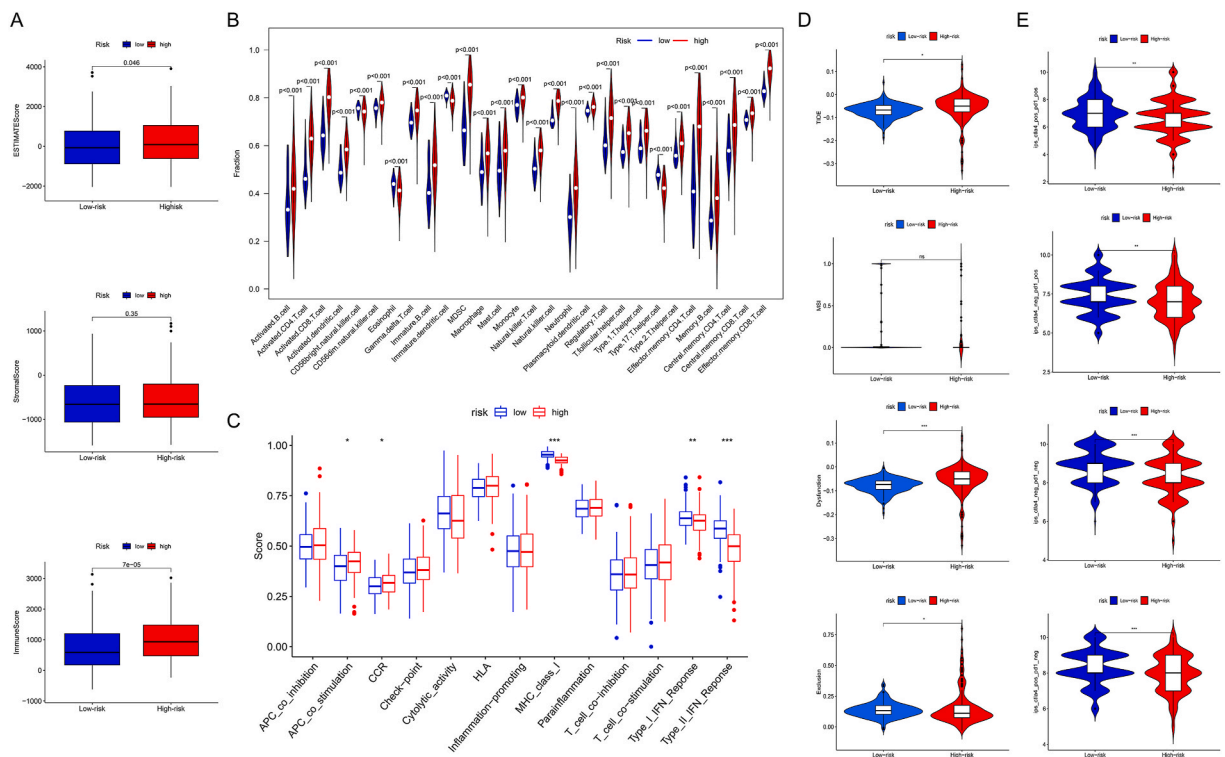


**Fig. 5.** Differences in Immune infiltration and TIDE scores between the high- and low-risk groups. (A) Differences in Estimate, immune, and stromal scores. (B) Differences of various immune cell types infiltration. (C) Differences in various immune functions. (D, E) Differences in TIDE, MSI, Exclusion, Dysfunction, and IPS scores among the high- and low-risk groups.

assess 28 types of immune cells in the two sub-groups. The levels of most immune cells were significantly higher in the high-risk group, except for CD56bright natural killer cells, eosinophils, immature dendritic cells, and Th17 cells (Fig. 5B). We also evaluated immune function scores and found that APC co-stimulation and C-C Motif Chemokine Receptor (CCR) scores were higher in the high-risk group, while MHC-I, type I IFN response, and type II IFN response scores were lower (Fig. 5C). Correlation analysis revealed that E2F2 and GTSE1 showed positive correlations with most immune cell types. RAD54L was negatively correlated with natural killer cells, monocytes, immature dendritic cells, and CD56bright natural killer cells but positively correlated with Th2 cells, Tregs, MDSCs, effector memory CD4<sup>+</sup> cells, central memory CD4<sup>+</sup> T cells, activated dendritic cells, activated CD8<sup>+</sup> T cells, and activated CD4<sup>+</sup> T cells. UBE2C showed positive associations with most immune cell types, except for neutrophils, immature dendritic cells, and eosinophils (Fig. S5). Immunotherapy holds promise as a treatment for cancer, and the TIDE score can aid oncologists in selecting patients who are more likely to benefit from immune checkpoint suppression therapy. Therefore, we calculated the TIDE scores for each ccRCC patient. As shown in Fig. 5D, the outcomes indicated that the low-risk group exhibited higher TIDE ( $p < 0.05$ ) and exclusion scores ( $p < 0.05$ ) but lower dysfunction scores ( $p < 0.001$ ) compared to the high-risk group. There was no significant difference observed in the MSI score. Another scoring system for predicting immunotherapy response was also introduced in our study. The IPS scores in the four phenotypes were consistently exhibited higher in the low-risk group but not in the high-risk group (Fig. 5E). Consequently, the low-risk group displayed higher total TIDE and IPS scores, suggesting that patients in this group may respond more effectively to treatment than those in the high-risk group.

### 3.6. Potential biological pathways enrichment analyzed by GO and KEGG

To identify the potential pathways involved, we conducted a screening of DEGs between the two subgroups. Our analysis revealed 222 down-regulated genes and 1086 up-regulated genes. Gene Ontology (GO) annotation analysis was performed, and it demonstrated that the biological pathways (BP) associated with cell division, organelle fission, nuclear division, mitotic nuclear division, and chromosome segregation were significantly enriched. In terms of cellular components (CC), the enrichment was observed in the collagen-containing extracellular matrix, chromosomal region, spindle, and microtubule. Furthermore, the molecular function (MF) analysis indicated enrichment in organic anion transmembrane transport activity, monooxygenase activity, and DNA replication origin binding (Fig. S6A). Additionally, the results from the Kyoto Encyclopedia of Genes and Genomes (KEGG) pathway analysis suggested that the DEGs were enriched in pathways such as the cell cycle, metabolism of xenobiotics by cytochrome P450, cellular senescence, and phagosome (Fig. S6B). These findings highlight the involvement of DEGs in cellular processes related to cell division and the cell cycle. In summary, our analysis of DEGs revealed their enrichment in pathways associated with cell division, organelle fission, nuclear division, mitotic nuclear division, and chromosome segregation, as well as in various cellular components and molecular functions. The KEGG pathway analysis further supported the involvement of these DEGs in critical cellular processes, emphasizing their significance in regulating cell cycle progression and related pathways.

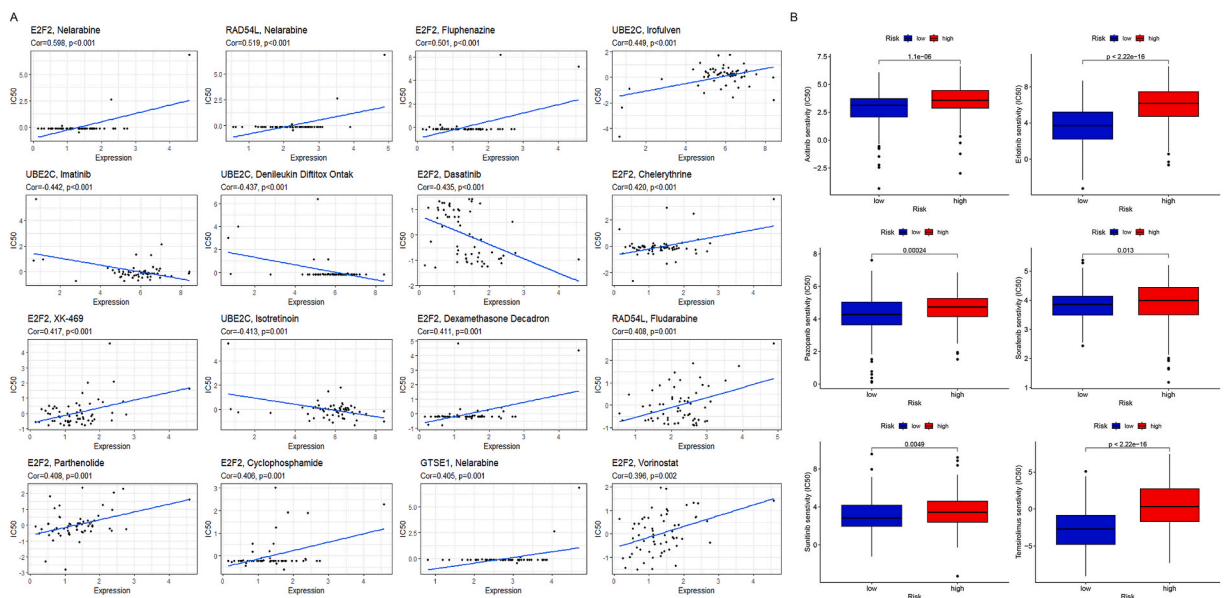


**Fig. 6.** Correlation analysis of gene expression and drug sensitivities. (A) The top 16 most associated relationships. (B) Comparison of sensitivities to Axitinib, Erlotinib, Pazopanib, Sorafenib, Sunitinib, and Temsirolimus between the high- and low-risk groups.

### 3.7. The differences in drug sensitivities between the two groups

To investigate the association between drug sensitivities and model genes, we utilized the CellMiner database, which encompasses a comprehensive collection of genomic and pharmacological information, including data from over 20,000 compounds tested on NCI-60 cell lines. We specifically examined 75 compounds that are currently under clinical trials, as well as 188 FDA-approved drugs. The analysis revealed the top 16 correlations, as depicted in Fig. 6A. Among the correlations, we found that E2F2 exhibited positive correlations with the IC50 values of Nelarabine, Fluphenazine, Chelerythrine, XK-469, Partheolide, and Vorinostat while showing a negative correlation with Dasatinib. RAD54L demonstrated a positive correlation with Nelarabine and Fludarabine. The expression of UBE2C displayed a positive correlation with Irofulven but a negative correlation with Imatinib, Denileukin Diftitox Ontak, and Isotretinoin. GTSE1 exhibited a positive correlation with Nelarabine. Furthermore, we employed the “pRRophetic” package to compare the sensitivities of six commonly used anticancer drugs between the two risk groups. The analysis indicated that the IC50 values of Axitinib, Erlotinib, Pazopanib, Sorafenib, Sunitinib, and Temsirolimus were higher in the low-risk group (Fig. 6B). This finding suggests that our prognostic signature is not only associated with patient outcomes but also linked to responses to chemotherapy treatment. Consequently, our signature may contribute to more precise drug selection for ccRCC patients. Overall, by leveraging the CellMiner database and utilizing the “pRRophetic” package, we identified correlations between drug sensitivities and model genes, providing insights into potential therapeutic options for ccRCC patients based on their risk profiles.

### 3.8. Two distinct clusters were identified based on the 4 prognostic GMCRGs

To gain further insights into potential subtypes among ccRCC patients, we employed a consistent unsupervised methodology based on the expression profiles of four GMCRGs. The clustering results demonstrated that when the number of subtypes ( $k$ ) was set to two, the clustering was the most stable (Fig. 7A, B). The range of fluctuation in the Cumulative Distribution Function (CDF) curves was minimal at the consensus index of 0.2–0.6 for  $k = 2$ , indicating a robust clustering outcome. Additionally, PCA and t-SNE plots further confirmed the distinct separation between the two clusters (Fig. 7C, D). Survival analysis revealed that patients in Cluster 2 exhibited a better survival rate compared to those in Cluster 1 (Fig. 7E). Furthermore, GSVA uncovered enriched pathways in each cluster. Cluster 2 displayed enrichment in cell cycle regulation, RNA polymerase activity, RNA degradation, nucleotide excision repair, and ubiquitin-mediated proteolysis. On the other hand, cluster 1 exhibited enrichment in metabolism-related pathways, including linoleic acid metabolism, arachidonic acid metabolism, retinol metabolism, fatty acid metabolism, and nitrogen metabolism (Fig. S7). Moreover, in terms of drug sensitivities, cluster 2 demonstrated higher sensitivity to the six common drugs: Axitinib, Erlotinib, Pazopanib, Sunitinib, and Temsirolimus (Fig. 7F). This finding suggests that cluster 2 patients may potentially benefit more from these drugs. In summary, our analysis based on the expression profiles of the four GMCRGs identified two distinct clusters within ccRCC patients. These clusters demonstrated differential survival outcomes, enriched biological pathways, and varying drug sensitivities. We further estimated the TIDE and IPS scores of the two clusters for predicting immunotherapy response. The TIDE and dysfunction scores of the cluster2 group were slightly higher compared to the cluster1 ( $p < 0.05$ ), and the cluster1 exhibited higher exclusion scores ( $p < 0.05$ ) (Fig. 7G). As

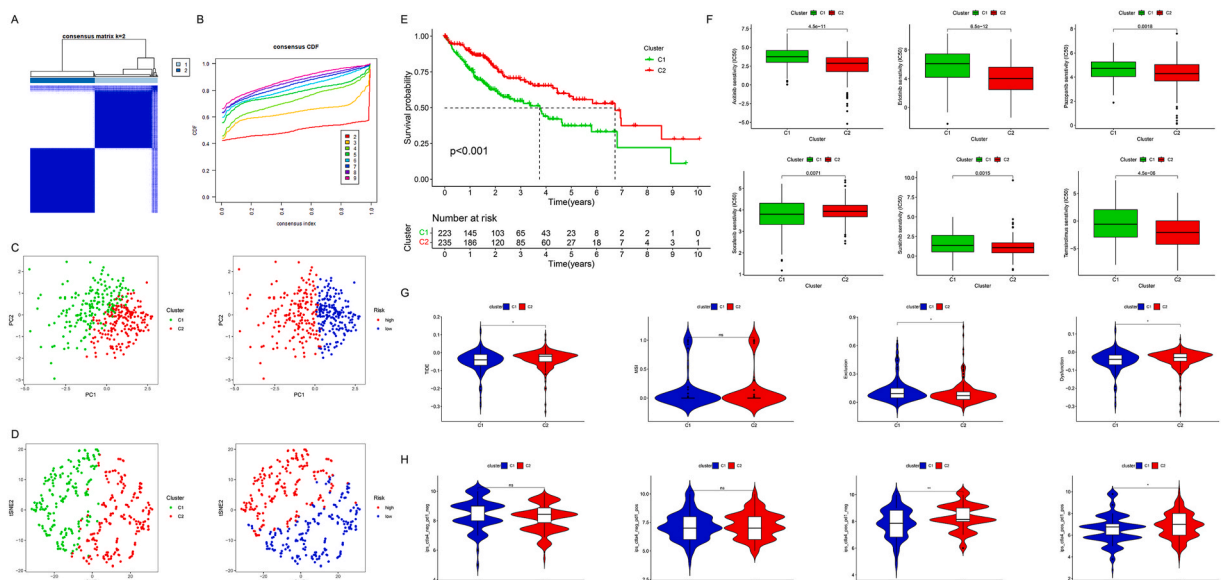
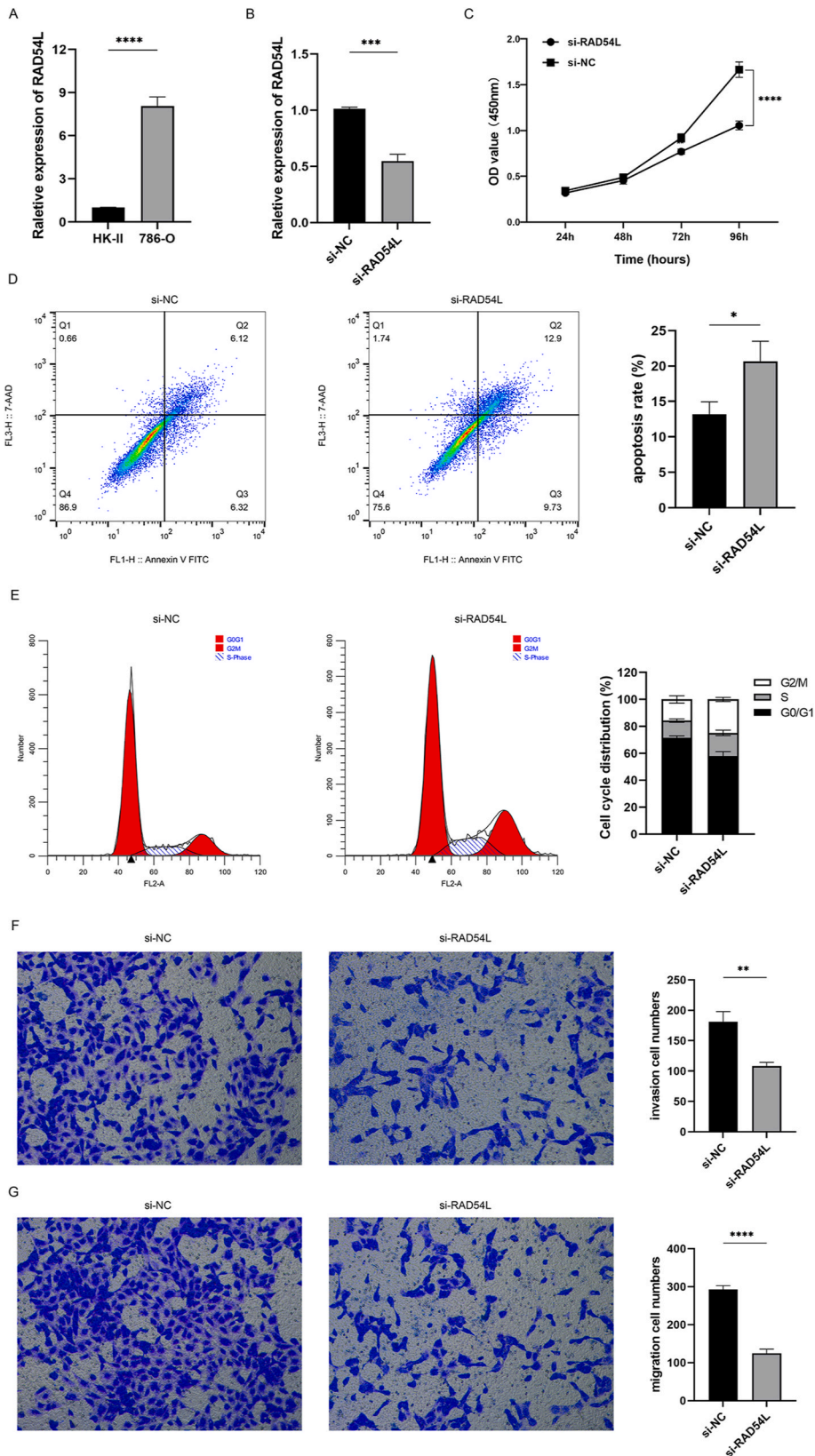


**Fig. 7.** Clustering ccRCC patients into different subtypes based on GMCRGs. (A) Consensus clustering matrix ( $k = 2$ ). (B) Cumulative distribution function (CDF) curves. PCA (C) and t-SNE (D) plots. (E) Survival curves of the two subtypes. (F) Comparison of sensitivities to Axitinib, Erlotinib, Pazopanib, Sorafenib, Sunitinib, and Temsirolimus between the two subgroups. (G, H) Differences in TIDE, MSI, Exclusion, Dysfunction, and IPS scores among the two clusters.



(caption on next page)

**Fig. 8. Knockdown of RAD54 by specific siRNA in the 786-O cell line. (A)** The expression level of RAD54L in HK-II and 786-O cell lines. **(B)** The expression level of RAD54L in the si-NC and si-RAD54L groups. **(C)** Cell proliferation curves assessing by CCK-8 method. **(D)** Cell apoptosis rate in the different groups. **(E)** Proportion of cell cycle. **(F, G)** Numbers of cell migration and invasion.

shown in Fig. 7H, patients in cluster2 with higher IPS scores in the phenotype of *ctla4\_pos\_pd1\_neg*, *ctla4\_pos\_pd1\_pos*, suggested that CTLA4 inhibitors alone or in combination with PD-1 inhibitors may be effective in cluster2 patients. These findings contribute to a better understanding of the heterogeneity within ccRCC and may have implications for personalized treatment strategies based on GMCRGs signature.

### 3.9. Knockdown of RAD54L suppresses tumor cell growth, invasion, and migration

The coefficient value for RAD54L was observed to be the highest in the model; however, there is currently no supporting evidence to elucidate its specific functional role in ccRCC. Firstly, we analyzed the expression of RAD54L via the scRNA sequencing GSE159115. A total of 33 clusters were identified and annotated into 8 different cell types (Fig. S8A, B). RAD54L was distributed in various cell types at low expression levels (Fig. S8C). To investigate further, we compared the expression levels of RAD54L between the HK-II and 786-O cell lines. The results indicated that the ccRCC cell line 786-O exhibited a significantly higher expression level of RAD54L compared to the normal cell line HK-II ( $p < 0.0001$ , Fig. 8A). Subsequently, transfection of the 786-O cell line with a siRNA molecule specifically targeting RAD54L, using Lipo3000, effectively reduced the expression level of RAD54L ( $p < 0.001$ , Fig. 8B). This siRNA-mediated knockdown of RAD54L resulted in significant impairment of cell proliferation ( $p < 0.0001$ , Fig. 8C). Additionally, the si-RAD54L group exhibited a higher rate of cell apoptosis compared to the si-NC group ( $20.68 \pm 2.831$  vs.  $13.17 \pm 1.781$ ,  $p = 0.0177$ , Fig. 8D). Furthermore, the knockdown of RAD54L led to an increase in the G2/M phase of the cell cycle and a reduction in the G0/G1 phase (Fig. 8E). Moreover, the si-RAD54L group demonstrated a noticeable decrease in both cell migration and invasion (Fig. 8F, G, respectively). In addition, we conducted GSEA analysis to investigate the potential signaling pathways in which RAD54L may be involved. Several metabolism-related pathways including 2-oxocarboxylic acid metabolism, citrate cycle (TCA cycle), and liponic acid metabolism (Fig. S8D), indicated that RAD54L may affect ccRCC progression via the above pathways. Collectively, these findings suggest that RAD54L had an oncogenic role in ccRCC progression.

## 4. Discussion

ccRCC is the most relevant cancer type in the kidney that is characterized by the presence of clear or pale cytoplasm within the cancer cells. This clear appearance is caused by the accumulation of abundant glycogen and lipids in the cytoplasm, giving the cells a clear or foamy appearance under a microscope. The most common genetic alteration observed in ccRCC is the loss of the Von Hippel-Lindau (VHL) tumor suppressor gene leads to the stabilization and accumulation of hypoxia-inducible factor (HIF), which promotes the growth of blood vessels and enhances cell survival. It is generally considered an aggressive form of kidney cancer for its potential to invade nearby tissues and metastasize to distant sites, such as the lungs, bones, or other organs. The prognosis for ccRCC depends on various factors, including the stage of the cancer at diagnosis, tumor size, extent of metastasis, and overall health of the patient. Early-stage ccRCC has a better prognosis compared to advanced-stage disease. With advancements in treatment options, including targeted therapies and immunotherapies, the prognosis for advanced-stage ccRCC has improved in recent years. However, the survival rate remains dissatisfactory.

The G2M checkpoint plays a significant role in safeguarding genomic stability by monitoring DNA integrity and preventing the progression of cells with damaged DNA into mitosis. Dysregulation or disruption of the G2M checkpoint pathways can have implications for cancer development. Cancer cells often exhibit alterations in cell cycle regulation, including disruptions in the G2M checkpoint. Mutations in genes that control cell cycle progression, such as p53, p21, or cyclins, can lead to faulty G2M checkpoint control. As a result, cancer cells may bypass the checkpoint and enter mitosis despite having damaged DNA. Assessing the status of the G2M checkpoint and related pathways can have diagnostic and therapeutic implications. Alterations in G2M checkpoint components or downstream signaling molecules may serve as biomarkers for predicting tumor behavior, treatment response, or prognosis. Additionally, targeting the G2M checkpoint and related pathways may represent therapeutic strategies to sensitize cancer cells to DNA-damaging treatments or to selectively induce cell death in ccRCC with compromised DNA repair capacity [21–23]. Understanding the association between the G2M checkpoint and cancer can provide insights into the underlying mechanisms driving tumorigenesis, help identify potential therapeutic targets, and guide the development of personalized treatment approaches.

In the present study, we constructed a prognostic model including four genes of E2F2, GTSE1, RAD54L, and UBE2C for ccRCC by integrative bioinformatic methods. E2F2 is a transcription factor that belongs to the E2F family of proteins and plays a crucial role in the regulation of the cell cycle and proliferation, specifically in the G1 to S phase transition. It regulates the expression of genes that are essential for DNA replication and cell division [24]. E2F2 forms complexes with other proteins, including members of the retinoblastoma protein (RB) family, to control the transcription of target genes [25]. E2F2 activity is tightly regulated by the RB family of proteins, including RB, p107, and p130 [26]. In its inactive state, E2F2 is bound to RB proteins, preventing its transcriptional activity. Upon phosphorylation of RB proteins by cyclin-dependent kinases (CDKs), E2F2 is released, allowing it to activate target gene expression [26]. Dysregulation of E2F2 activity can disrupt cell cycle control and contribute to abnormal cell proliferation, a hallmark of cancer. E2F2 has been implicated in cancer development and progression. Its aberrant activation or dysregulation has been observed in various types of cancers, including glioma [27], lung adenocarcinoma [28], colorectal cancer [27], and pancreatic ductal

adenocarcinoma [29]. In our study, we found that E2F2 was a risk factor and correlated to poor prognosis in ccRCC, the result was similar to the published articles [30,31]. Furthermore, E2F2 exhibited a positive association with various types of immune cells, indicating its potential involvement in regulating the immune cell cycle within ccRCC infiltration. Additionally, heightened E2F2 activity in malignant or stromal cells may also attract immune cells. However, further experiments are required to validate this hypothesis. Moreover, the expression level of E2F2 correlated with drug sensitivities, demonstrating positive correlations with IC50 values of Nelarabine, Fluphenazine, Chelerythrine, XK-469, Partheolde, and Vorinostat, while displaying a negative correlation with Dasatinib. Therefore, assessing the expression level of E2F2 in ccRCC tissue may be beneficial for personalized therapy. GTSE1, referred to as B99 or TSG24 represents a protein that is predominantly active in the G2 and S stages of the cell cycle. Its main role involves facilitating the smooth advancement of mitosis by controlling the dynamics of microtubules and guaranteeing the precise segregation of chromosomes [32]. Notably, GTSE1's involvement in these processes holds significance in the context of cancer development and progression [33–36]. GTSE1 interacts with the tumor suppressor protein p53, forming a complex that regulates p53 stability and function, and helps to sequester p53 in the cytoplasm, preventing its translocation to the nucleus and its activation as a transcription factor [37,38]. This interaction may contribute to the control of cell cycle progression and apoptosis. GTSE1 is also involved in the cellular response to DNA damage. It interacts with proteins involved in DNA repair, such as BRCA1 and RAD51, and contributes to the maintenance of genomic stability [32]. According to a study by Lei et al., the overexpression of GTSE1 in ccRCC is linked to unfavorable OS and resistance to cisplatin treatment. Conversely, the reduction of GTSE1 expression can impede the malignant advancement of ccRCC by suppressing cell proliferation, impeding cell cycle transition, mitigating migration and invasion capabilities, and increasing the sensitivity of ccRCC cells to cisplatin [39]. We found that the expression of GTSE1 was correlated with the IC50 of Nelarabine. In addition, the role of GTSE1 in epithelial-mesenchymal transition (EMT) was found to be significant, as it regulates the expression of Krüppel-like factor 4 (KLF4) [40]. Further research is needed to fully understand the complex mechanisms and functional implications of GTSE1 in cellular processes and its significance in cancer biology. UBE2C, also known as Ubiquitin-conjugating enzyme E2C, one of the ubiquitin-conjugating enzymes that are responsible for protein degradation, plays a crucial role in transferring ubiquitin molecules to target proteins, marking them for degradation by the proteasome. UBE2C levels increase during the G2/M phase transition, contributing to the proper progression of mitosis. Its expression levels are tightly controlled throughout different phases of the cell cycle. UBE2C levels increase during the G2/M phase transition, contributing to the proper progression of mitosis [41,42]. UBE2C also plays a significant role in mitotic progression by controlling the degradation of key proteins involved in cell division [43]. UBE2C has been found to be upregulated in several types of cancers, including breast, lung, colorectal, and ovarian cancers. Increased UBE2C expression has been associated with poor prognosis, advanced disease stage, and resistance to chemotherapy [44,45]. It may play a role in promoting cell proliferation, survival, and tumor growth. Additionally, it appears that UBE2C is closely linked to immune cell infiltration in ccRCC. While the expression of UBE2C showed positive correlations with several anti-cancer immune cell types, including activated CD4<sup>+</sup> and CD8<sup>+</sup> T cells, as well as gamma delta T cells, it also demonstrated a strong association with regulatory T cells (Tregs) and myeloid-derived suppressor cells (MDSCs). These cell types are known for their role in immune suppression within the cancer microenvironment [46,47]. The contradictory role of UBE2C in immune infiltration remains to be explored. Given its association with cancer progression, drug resistance, and immune microenvironment, UBE2C has emerged as a potential therapeutic target. Inhibition of UBE2C activity or targeted degradation of UBE2C protein could provide a strategy for developing novel anticancer therapies. RAD54L is a member of the SWI2/SNF2 family of DNA-dependent ATPases and is involved in DNA repair and recombination pathways. It functions in the homologous recombination (HR) pathway, which is responsible for repairing DNA double-strand breaks and maintaining genomic stability [48]. RAD54L interacts with various proteins involved in DNA repair and recombination, including RAD51, RAD52, and BRCA2 [49–51]. These interactions facilitate the assembly of protein complexes at DNA damage sites and enhance the efficiency of HR-mediated repair processes. More and more evidence suggests that dysregulation or mutations in RAD54L are associated with poor prognosis and increased tumor aggressiveness [52–55]. Alterations in RAD54L expression or function can impair DNA repair processes, leading to genomic instability and an increased susceptibility to cancer. RAD54L variants have also been linked to conditions such as Fanconi anemia, a rare inherited disorder characterized by DNA repair defects [56,57]. According to Peng et al., RAD54L was identified as a significant model gene associated with the prognosis of ccRCC, highlighting its role in DNA damage repair [58]. However, there is no functional result to reveal its role in ccRCC. In the present study, we constructed small interference RNA to specifically knock down RAD54L in ccRCC cell line 786-O. Our findings demonstrated that the down-regulation of RAD54L in 786-O cells resulted in the inhibition of cell growth, migration, and invasion. Additionally, there was an observed increase in the level of cell apoptosis, and knockdown of RAD54L led to the arrest of cells in the G2/M phase of the cell cycle. Mun et al. reported that E2F1 as a transcriptional factor that influences RAD54L plays a significant role in the development and advancement of bladder cancer [59]. E2F2's function is similar to E2F1, while it was one of the model genes in our study, whether it may affect RAD54L remains unknown. Further studies were needed.

Despite successfully constructing an effective model and conducting experimental verification in the present study, it is imperative to acknowledge certain limitations. Firstly, there is a lack of independent validation of the findings. Additional datasets or experimental validation, either *in vitro* or *in vivo*, would bolster the robustness of the identified prognostic genes. Additionally, while the study provided insights into potential biological pathways associated with these genes, further experimental studies are necessary to elucidate the underlying biological mechanisms. Understanding how these genes regulate cell cycle progression, tumor growth, and response to therapy would facilitate the development of targeted therapeutic strategies for ccRCC. Furthermore, while the functional characterization of RAD54L using cell line-based assays offers valuable insights into its potential role in ccRCC progression, caution should be exercised when extrapolating these findings to clinical settings. Cell line models may not fully replicate the complexity of tumor behavior *in vivo*. Therefore, further validation in preclinical models or patient-derived samples is warranted to confirm the functional relevance of RAD54L in ccRCC.

To summarize, we developed a prognostic model related to the G2M checkpoint, specifically involving E2F2, GTSE1, RAD54L, and UBE2C. This model enables the prediction of OS in ccRCC using both single-cell RNA sequencing and bulk-sequencing data. Additionally, we created a nomogram and identified subtypes specific to ccRCC based on the four genes. The genes within the model not only demonstrate correlations with immune infiltration but also exhibit varying sensitivities to different drugs. These findings hold significant predictive value and hold promise for clinical applications in glioma therapy.

## Fundings

The study was funded by the Science and Technology Planning Project of Guangzhou City (Grant No. 202201020582), 3D Printing Scientific Research Foundation of Guangdong Second Provincial General Hospital (Grant No.3D-D2020021), Medical Science and Technology Research Foundation of Guangdong Province (Grant No.B2022303), National Natural Science Foundation of China (Grant No. 82302304), the Guangzhou Science and Technology Plan Project (Grant No. 2024A04J4159), the Doctoral Workstation Foundation of Guangdong Second Provincial General Hospital (Grant No. 2022BSGZ011), and the Elevate Engineering Foundation of Guangdong Second Provincial General Hospital (Grant No. TJGC2022009).

## Data availability statement

The public cohort datasets collected in the present study are available online on the Cancer Genome Atlas (TCGA) and Gene Expression Omnibus (GEO) websites. Additional data could be available upon request to the corresponding author.

## CRedit authorship contribution statement

**Zhenwei Wang:** Writing – original draft. **Zongtai Zheng:** Software, Investigation. **Bangqi Wang:** Visualization, Investigation. **Changxin Zhan:** Investigation. **Xuefeng Yuan:** Data curation. **Xiaoqi Lin:** Investigation. **Qifan Xin:** Methodology. **Zhihui Zhong:** Writing – review & editing. **Xiaofu Qiu:** Supervision, Funding acquisition.

## Declaration of competing interest

The authors declare the following financial interests/personal relationships which may be considered as potential competing interests: Zhenwei Wang reports statistical analysis was provided by Gaozhou People's Government. Zhenwei Wang reports a relationship with The People's Hospital of Gaozhou that includes: non-financial support. We declare that we have no financial and personal relationships with other people or organizations that can inappropriately influence our work, there is no professional or other personal interest of any nature or kind in any product, service and/or company that could be constructed as influencing the position presented in, or the review of, in the manuscript entitled. If there are other authors, they declare that they have no known competing financial interests or personal relationships that could have appeared to influence the work reported in this paper.

## Appendix A. Supplementary data

Supplementary data to this article can be found online at <https://doi.org/10.1016/j.heliyon.2024.e29289>.

## References

- [1] L. Bukavina, K. Bensalah, F. Bray, M. Carlo, B. Challacombe, J.A. Karam, W. Kassouf, T. Mitchell, R. Montironi, T. O'Brien, V. Panebianco, G. Scelo, B. Shuch, H. van Poppel, C.D. Blosser, S.P. Psutka, Epidemiology of renal cell carcinoma: 2022 update, *Eur. Urol.* 82 (2022) 529–542, <https://doi.org/10.1016/j.eururo.2022.08.019>.
- [2] J.J. Hsieh, M.P. Purdue, S. Signoretti, C. Swanton, L. Albiges, M. Schmidinger, D.Y. Heng, J. Larkin, V. Ficarra, Renal cell carcinoma, *Nat. Rev. Dis. Prim.* 3 (2017) 17009, <https://doi.org/10.1038/nrdp.2017.9>.
- [3] M.B. Atkins, N.M. Tannir, Current and emerging therapies for first-line treatment of metastatic clear cell renal cell carcinoma, *Cancer Treat Rev.* 70 (2018) 127–137, <https://doi.org/10.1016/j.ctrv.2018.07.009>.
- [4] E. Jonasch, C.L. Walker, W.K. Rathmell, Clear cell renal cell carcinoma ontogeny and mechanisms of lethality, *Nat. Rev. Nephrol.* 17 (2021) 245–261, <https://doi.org/10.1038/s41581-020-00359-2>.
- [5] P. Makhov, S. Joshi, P. Ghatalia, A. Kutikov, R.G. Uzzo, V.M. Kolenko, Resistance to systemic therapies in clear cell renal cell carcinoma: mechanisms and management strategies, *Mol. Cancer Ther.* 17 (2018) 1355–1364, <https://doi.org/10.1158/1535-7163.MCT-17-1299>.
- [6] J. Yang, K. Wang, Z. Yang, Treatment strategies for clear cell renal cell carcinoma: past, present and future, *Front. Oncol.* 13 (2023) 1133832, <https://doi.org/10.3389/fonc.2023.1133832>.
- [7] A. Sancar, L.A. Lindsey-Boltz, K. Unsal-Kaçmaz, S. Linn, Molecular mechanisms of mammalian DNA repair and the DNA damage checkpoints, *Annu. Rev. Biochem.* 73 (2004) 39–85, <https://doi.org/10.1146/annurev.biochem.73.011303.073723>.
- [8] M. Löbrich, P.A. Jeggo, The impact of a negligent G2/M checkpoint on genomic instability and cancer induction, *Nat. Rev. Cancer* 7 (2007) 861–869, <https://doi.org/10.1038/nrc2248>.
- [9] G.R. Stark, W.R. Taylor, Control of the G2/M transition, *Mol. Biotechnol.* 32 (2006) 227–248, <https://doi.org/10.1385/MB:32:3:227>.
- [10] K. Engeland, Cell cycle arrest through indirect transcriptional repression by p53: I have a DREAM, *Cell Death Differ.* 25 (2018) 114–132, <https://doi.org/10.1038/cdd.2017.172>.

- [11] N. Barnaba, J.R. LaRocque, Targeting cell cycle regulation via the G2-M checkpoint for synthetic lethality in melanoma, *Cell Cycle* 20 (2021) 1041–1051, <https://doi.org/10.1080/15384101.2021.1922806>.
- [12] M. Oshi, H. Takahashi, Y. Tokumaru, L. Yan, O.M. Rashid, R. Matsuyama, I. Endo, K. Takabe, G2M cell cycle pathway score as a prognostic biomarker of metastasis in estrogen receptor (ER)-Positive breast cancer, *Int. J. Mol. Sci.* 21 (2020), <https://doi.org/10.3390/ijms21082921>.
- [13] X. Lv, Y. Zhao, L. Zhang, S. Zhou, B. Zhang, Q. Zhang, L. Jiang, X. Li, H. Wu, L. Zhao, M. Wei, M. He, Development of a novel gene signature in patients without *Helicobacter pylori* infection gastric cancer, *J. Cell. Biochem.* 121 (2020) 1842–1854, <https://doi.org/10.1002/jcb.29419>.
- [14] M. Oshi, S. Newman, Y. Tokumaru, L. Yan, R. Matsuyama, I. Endo, M.H.G. Katz, K. Takabe, High G2M pathway score pancreatic cancer is associated with worse survival, particularly after margin-positive (R1 or R2) resection, *Cancers* 12 (2020), <https://doi.org/10.3390/cancers12102871>.
- [15] S.E. Morgan, M.B. Kastan, p53 and ATM: cell cycle, cell death, and cancer, *Adv. Cancer Res.* 71 (1997) 1–25, [https://doi.org/10.1016/s0065-230x\(08\)60095-0](https://doi.org/10.1016/s0065-230x(08)60095-0).
- [16] H.L. Smith, H. Southgate, D.A. Tweddle, N.J. Curtin, DNA damage checkpoint kinases in cancer, *Expert Rev. Mol. Med.* 22 (2020) e2, <https://doi.org/10.1017/erm.2020.3>.
- [17] M. Oshi, A. Patel, L. Le, Y. Tokumaru, L. Yan, R. Matsuyama, I. Endo, K. Takabe, G2M checkpoint pathway alone is associated with drug response and survival among cell proliferation-related pathways in pancreatic cancer, *Am. J. Cancer Res.* 11 (2021) 3070–3084.
- [18] C.-X. Deng, BRCA1: cell cycle checkpoint, genetic instability, DNA damage response and cancer evolution, *Nucleic Acids Res.* 34 (2006) 1416–1426, <https://doi.org/10.1093/nar/gkl010>.
- [19] N. Bucher, C.D. Britten, G2 checkpoint abrogation and checkpoint kinase-1 targeting in the treatment of cancer, *Br. J. Cancer* 98 (2008) 523–528, <https://doi.org/10.1038/sj.bjc.6604208>.
- [20] K. Liu, M. Zheng, R. Lu, J. Du, Q. Zhao, Z. Li, Y. Li, S. Zhang, The role of CDC25C in cell cycle regulation and clinical cancer therapy: a systematic review, *Cancer Cell Int.* 20 (2020) 213, <https://doi.org/10.1186/s12935-020-01304-w>.
- [21] B. Li, Y.-J. Gao, X.-Y. Wu, J. Cui, Y. Long, J.-L. Xu, D.-G. Ding, Tumor-initiating cells contribute to radiation resistance in primary human renal clear cell carcinomas by activating the DNA damage checkpoint response, *Oncol. Lett.* 14 (2017) 3261–3267, <https://doi.org/10.3892/ol.2017.6504>.
- [22] X.-W. Pan, L. Chen, Y. Hong, D.-F. Xu, X. Liu, L. Li, Y. Huang, L.-M. Cui, S.-S. Gan, Q.-W. Yang, H. Huang, F.-J. Qu, J.-Q. Ye, L.-H. Wang, X.-G. Cui, EIF3D silencing suppresses renal cell carcinoma tumorigenesis via inducing G2/M arrest through downregulation of Cyclin B1/CDK1 signaling, *Int. J. Oncol.* 48 (2016) 2580–2590, <https://doi.org/10.3892/ijo.2016.3459>.
- [23] X. Huang, Y. Huang, Z. Lv, T. Wang, H. Feng, H. Wang, S. Du, S. Wu, D. Shen, C. Wang, H. Li, B. Wang, X. Ma, X. Zhang, Loss of cell division cycle-associated 5 promotes cell apoptosis by activating DNA damage response in clear cell renal cell carcinoma, *Int. J. Oncol.* 61 (2022), <https://doi.org/10.3892/ijo.2022.5377>.
- [24] Q. Liu, C. Song, J. Li, M. Liu, L. Fu, J. Jiang, Z. Zeng, H. Zhu, E2F2 enhances the chemoresistance of pancreatic cancer to gemcitabine by regulating the cell cycle and upregulating the expression of RRM2, *Med. Oncol.* 39 (2022) 124, <https://doi.org/10.1007/s12032-022-01715-x>.
- [25] U. Laresgoiti, A. Apraiz, M. Olea, J. Mitxelena, N. Osinalde, J.A. Rodriguez, A. Fullaondo, A.M. Zubiaga, E2F2 and CREB cooperatively regulate transcriptional activity of cell cycle genes, *Nucleic Acids Res.* 41 (2013) 10185–10198, <https://doi.org/10.1093/nar/gkt821>.
- [26] C. Chen, Q. Zheng, S. Pan, W. Chen, J. Huang, Y. Cao, Y. Tu, Z. Li, C. Yu, Z. Jie, The RNA-binding protein NLFPE promotes gastric cancer growth and metastasis through E2F2, *Front. Oncol.* 11 (2021) 677111, <https://doi.org/10.3389/fonc.2021.677111>.
- [27] Y. Shang, Y. Zhang, J. Liu, L. Chen, X. Yang, Z. Zhu, D. Li, Y. Deng, Z. Zhou, B. Lu, C.-G. Fu, Decreased E2F2 expression correlates with poor prognosis and immune infiltrates in patients with colorectal cancer, *J. Cancer* 13 (2022) 653–668, <https://doi.org/10.7150/jca.61415>.
- [28] K. Du, S. Sun, T. Jiang, T. Liu, X. Zuo, X. Xia, X. Liu, Y. Wang, Y. Bu, E2F2 promotes lung adenocarcinoma progression through B-Myb- and FOXM1-facilitated core transcription regulatory circuitry, *Int. J. Biol. Sci.* 18 (2022) 4151–4170, <https://doi.org/10.7150/ijbs.72386>.
- [29] Y. Yang, Z. Guo, W. Chen, X. Wang, M. Cao, X. Han, K. Zhang, B. Teng, J. Cao, W. Wu, P. Cao, C. Huang, Z. Qiu, M2 macrophage-derived exosomes promote angiogenesis and growth of pancreatic ductal adenocarcinoma by targeting E2F2, *Mol. Ther.* 29 (2021) 1226–1238, <https://doi.org/10.1016/j.ymthe.2020.11.024>.
- [30] Z.-G. Liu, J. Su, H. Liu, X.-J. Yang, X. Yang, Y. Wei, X.-Y. Zhu, Y. Song, X.-C. Zhao, H.-L. Guo, Comprehensive bioinformatics analysis of the E2F family in human clear cell renal cell carcinoma, *Oncol. Lett.* 24 (2022) 351, <https://doi.org/10.3892/ol.2022.13471>.
- [31] X. Jing, G. Xu, Y. Gong, J. LiLingfengWu, W. Zhu, Y. He, Z. Li, S. Pan, A five-gene methylation signature predicts overall survival of patients with clear cell renal cell carcinoma, *J. Clin. Lab. Anal.* 35 (2021) e24031, <https://doi.org/10.1002/jcla.24031>.
- [32] S. Bendre, A. Rondelet, C. Hall, N. Schmidt, Y.-C. Lin, G.J. Brouhard, A.W. Bird, GTSE1 tunes microtubule stability for chromosome alignment and segregation by inhibiting the microtubule depolymerase MCAK, *J. Cell Biol.* 215 (2016) 631–647, <https://doi.org/10.1083/jcb.201606081>.
- [33] V.V. Subhash, S.H. Tan, W.L. Tan, M.S. Yeo, C. Xie, F.Y. Wong, Z.Y. Kiat, R. Lim, W.P. Yong, GTSE1 expression represses apoptotic signaling and confers cisplatin resistance in gastric cancer cells, *BMC Cancer* 15 (2015) 550, <https://doi.org/10.1186/s12885-015-1550-0>.
- [34] W. Lai, W. Zhu, X. Li, Y. Han, Y. Wang, Q. Leng, M. Li, X. Wen, GTSE1 promotes prostate cancer cell proliferation via the SP1/FOXM1 signaling pathway, *Lab. Invest.* 101 (2021) 554–563, <https://doi.org/10.1038/s41374-020-00510-4>.
- [35] F. Wu, Y. Mao, T. Ma, X. Wang, H. Wei, T. Wang, J. Wang, Y. Zhang, CTP1S inhibition suppresses proliferation and migration in colorectal cancer cells, *Cell Cycle* 21 (2022) 2563–2574, <https://doi.org/10.1080/15384101.2022.2105084>.
- [36] C. Xie, W. Xiang, H. Shen, J. Shen, GTSE1 is possibly involved in the DNA damage repair and cisplatin resistance in osteosarcoma, *J. Orthop. Surg. Res.* 16 (2021) 713, <https://doi.org/10.1186/s13018-021-02859-8>.
- [37] X.S. Liu, H. Li, B. Song, X. Liu, Polo-like kinase 1 phosphorylation of G2 and S-phase-expressed 1 protein is essential for p53 inactivation during G2 checkpoint recovery, *EMBO Rep.* 11 (2010) 626–632, <https://doi.org/10.1038/embor.2010.90>.
- [38] F. Lin, Y.-J. Xie, X.-K. Zhang, T.-J. Huang, H.-F. Xu, Y. Mei, H. Liang, H. Hu, S.-T. Lin, F.-F. Luo, Y.-H. Lang, L.-X. Peng, C.-N. Qian, B.-J. Huang, GTSE1 is involved in breast cancer progression in p53 mutation-dependent manner, *J. Exp. Clin. Cancer Res.* 38 (2019) 152, <https://doi.org/10.1186/s13046-019-1157-4>.
- [39] P. Lei, M. Zhang, Y. Li, Z. Wang, High GTSE1 expression promotes cell proliferation, metastasis and cisplatin resistance in ccRCC and is associated with immune infiltrates and poor prognosis, *Front. Genet.* 14 (2023) 996362, <https://doi.org/10.3389/fgene.2023.996362>.
- [40] W. Chen, H. Wang, Y. Lu, Y. Huang, Y. Xuan, X. Li, T. Guo, C. Wang, D. Lai, S. Wu, W. Zhao, H. Mai, H. Li, B. Wang, X. Ma, X. Zhang, GTSE1 promotes tumor growth and metastasis by attenuating of KLF4 expression in clear cell renal cell carcinoma, *Lab. Invest.* 102 (2022) 1011–1022, <https://doi.org/10.1038/s41374-022-00797-5>.
- [41] H. Wang, C. Zhang, A. Rorick, D. Wu, M. Chiu, J. Thomas-Ahner, Z. Chen, H. Chen, S.K. Clinton, K.K. Chan, Q. Wang, CCI-779 inhibits cell-cycle G2-M progression and invasion of castration-resistant prostate cancer via attenuation of UBE2C transcription and mRNA stability, *Cancer Res.* 71 (2011) 4866–4876, <https://doi.org/10.1158/0008-5472.CAN-10-4576>.
- [42] P. Nicolau-Neto, A. Palumbo, M. De Martino, F. Esposito, T. de Almeida Simão, A. Fusco, L.E. Nasciutti, N. Meireles Da Costa, L.F. Ribeiro Pinto, UBE2C is a transcriptional target of the cell cycle regulator FOXM1, *Genes* 9 (2018), <https://doi.org/10.3390/genes9040188>.
- [43] P. Bavi, S. Uddin, M. Ahmed, Z. Jehan, R. Bu, J. Abubaker, M. Sultana, N. Al-Sanea, A. Abduljabbar, L.H. Ashari, S. Alhomoud, F. Al-Dayel, S. Prabhakaran, A. R. Hussain, K.S. Al-Kuraya, Bortezomib stabilizes mitotic cyclins and prevents cell cycle progression via inhibition of UBE2C in colorectal carcinoma, *Am. J. Pathol.* 178 (2011) 2109–2120, <https://doi.org/10.1016/j.ajpath.2011.01.034>.
- [44] H. Dastsooz, M. Cereda, D. Donna, S. Oliviero, A comprehensive bioinformatics analysis of UBE2C in cancers, *Int. J. Mol. Sci.* 20 (2019), <https://doi.org/10.3390/ijms20092228>.
- [45] L. Yuan, Z. Yang, J. Zhao, T. Sun, C. Hu, Z. Shen, G. Yu, Pan-cancer bioinformatics analysis of gene UBE2C, *Front. Genet.* 13 (2022) 893358, <https://doi.org/10.3389/fgene.2022.893358>.
- [46] F. García-Arévalo, A.G. Leija-Montoya, J. González-Ramírez, M. Isordia-Espinoza, I. Serafin-Higuera, D.M. Fuchen-Ramos, J.G. Vazquez-Jimenez, N. Serafin-Higuera, Modulation of myeloid-derived suppressor cell functions by oral inflammatory diseases and important oral pathogens, *Front. Immunol.* 15 (2024) 1349067, <https://doi.org/10.3389/fimmu.2024.1349067>.

- [47] D. Qin, Y. Zhang, P. Shu, Y. Lei, X. Li, Y. Wang, Targeting tumor-infiltrating tregs for improved antitumor responses, *Front. Immunol.* 15 (2024) 1325946, <https://doi.org/10.3389/fimmu.2024.1325946>.
- [48] S.J. Ceballos, W.-D. Heyer, Functions of the Snf2/Swi2 family Rad54 motor protein in homologous recombination, *Biochim. Biophys. Acta* 1809 (2011) 509–523, <https://doi.org/10.1016/j.bbagr.2011.06.006>.
- [49] H. Li, H. Zhuang, T. Gu, G. Li, Y. Jiang, S. Xu, Q. Zhou, RAD54L promotes progression of hepatocellular carcinoma via the homologous recombination repair pathway, *Funct. Integr. Genomics* 23 (2023) 128, <https://doi.org/10.1007/s10142-023-01060-w>.
- [50] S. Wessman, B.B. Fuentes, T. Törngren, A. Kvist, G. Kokaraki, H. Menkens, E. Hjerpe, Y. Hugo, T.B. Petta, Å. Borg, J.W. Carlson, Precision oncology of high-grade ovarian cancer defined through targeted sequencing, *Cancers* 13 (2021), <https://doi.org/10.3390/cancers13205240>.
- [51] P. Selemenakis, N. Sharma, M.E. Uhrig, J. Katz, Y. Kwon, P. Sung, C. Wiese, RAD51AP1 and RAD54L can underpin two distinct RAD51-dependent routes of DNA damage repair via homologous recombination, *Front. Cell Dev. Biol.* 10 (2022) 866601, <https://doi.org/10.3389/fcell.2022.866601>.
- [52] C. Liu, W. Ren, Z. Zhang, J. Guan, DNA repair/recombination protein 54L promotes the progression of lung adenocarcinoma by activating mTORC1 pathway, *Hum. Cell* 36 (2023) 421–433, <https://doi.org/10.1007/s13577-022-00832-z>.
- [53] Y. Wang, T. Zhou, H. Chen, S. Wen, P. Dao, M. Chen, Rad54L promotes bladder cancer progression by regulating cell cycle and cell senescence, *Med. Oncol.* 39 (2022) 185, <https://doi.org/10.1007/s12032-022-01751-7>.
- [54] I.P.N. Bong, C.C. Ng, N. Othman, E. Esa, Gene expression profiling and in vitro functional studies reveal RAD54L as a potential therapeutic target in multiple myeloma, *Genes Genomics* 44 (2022) 957–966, <https://doi.org/10.1007/s13258-022-01272-7>.
- [55] Y. Tong, D. Merino, B. Nimmervoll, K. Gupta, Y.-D. Wang, D. Finkelstein, J. Dalton, D.W. Ellison, X. Ma, J. Zhang, D. Malkin, R.J. Gilbertson, Cross-species genomics identifies TAF12, NFYC, and RAD54L as choroid plexus carcinoma oncogenes, *Cancer Cell* 27 (2015) 712–727, <https://doi.org/10.1016/j.ccell.2015.04.005>.
- [56] A. Brannvoll, X. Xue, Y. Kwon, S. Kompocholi, A.K.W. Simonsen, K.S. Viswalingam, L. Gonzalez, I.D. Hickson, V.H. Oestergaard, H.W. Mankouri, P. Sung, M. Lisby, The ZGRF1 helicase promotes recombinational repair of replication-blocking DNA damage in human cells, *Cell Rep.* 32 (2020) 107849, <https://doi.org/10.1016/j.celrep.2020.107849>.
- [57] R. Mjelle, S.A. Hegre, P.A. Aas, G. Slupphaug, F. Drablos, P. Saetrom, H.E. Krokan, Cell cycle regulation of human DNA repair and chromatin remodeling genes, *DNA Repair* 30 (2015) 53–67, <https://doi.org/10.1016/j.dnarep.2015.03.007>.
- [58] L. Peng, J. Liang, Q. Wang, G. Chen, A DNA damage repair gene signature associated with immunotherapy response and clinical prognosis in clear cell renal cell carcinoma, *Front. Genet.* 13 (2022) 798846, <https://doi.org/10.3389/fgene.2022.798846>.
- [59] J.-Y. Mun, S.-W. Baek, W.Y. Park, W.-T. Kim, S.-K. Kim, Y.-G. Roh, M.-S. Jeong, G.-E. Yang, J.-H. Lee, J.W. Chung, Y.H. Choi, I.-S. Chu, S.-H. Leem, E2F1 promotes progression of bladder cancer by modulating RAD54L involved in homologous recombination repair, *Int. J. Mol. Sci.* 21 (2020), <https://doi.org/10.3390/ijms21239025>.